Effects of catheter, stenosis and thrombosis in non-Newtonian blood flow through narrow arteries with clinical applications - A mathematical model

Afiqah Wajihah S., D.S. Sankar, Atulya K Nagar
Applied Mathematics and Economics Programme Area
School of Applied Sciences and Mathematics
Universiti Teknologi Brunei
Jalan Tungku Link, Gadong BE1410,
Bandar Seri Begawan, Brunei Darussalam

School of Mathematics
Computer Science and Engineering
Liverpool Hope University
Hope Park, Liverpool L16 9JD, United Kingdom

p20181013@student.utb.edu.bn , duraisamy.sankar@utb.edu.bn,
naragara@hope.ac.uk

Keywords: Carreau fluid model; Copper Nanoparticles; Stenosed artery; Thrombosis; Catheterization; Clinical Applications.
*Corresponding Author: D S Sankar: duraisamy.sankar@utb.edu.bn

Abstract

This study analyses the rheological characteristics of non-Newtonian Carreau fluid model for nanoparticles suspended flow of blood through constricted arteries in the presence of stenosis, thrombosis and catheters. Analytical expressions, such as, velocity distribution, temperature, pressure gradient, wall shear stress and resistive impedance to flow are obtained by implementing the perturbation method and through the extensive use of MATLAB and MATHEMATICA programming tools, the results are presented

graphically and tabularly. It is found that temperature of the fluid lessens with the increase in stenosis shape parameter and depth of stenosis which results in the reduction of flow of blood in the artery. It is discovered that a rise in Weissenberg number results in the decrease of fluid's velocity and skin friction. The magnitude of resistance to blood flow reduces with the upsurge of flow rate and stenosis shape parameter and the reverse character is recognized when Weissenberg number, the depth and axial displacement of blood clot increases. When the angioplasty catheter of radius 0.3 is inserted to the clear the constrictions in the artery, the resistance to flow surges considerably in the range of 6.75-8.78 when the stenosis position extends in the axial direction from 0.1 to 0.3. It is also recorded that when the catheter guidewire radius is 0.18, the pressure gradient in blood flow is found to vary in the range of 1.21-1.43 when the axial variable z varies from 0.2 to 0.8 and it decreases from 1.36-1.32 when the blood clot position displaces from 0.2 to 0.6.

Keywords: Carreau fluid model; Copper nanoparticles; Stenosed artery; Thrombosis; Catheterization; Clinical applications.

*Corresponding Author: D S Sankar: duraisamy.sankar@utb.edu.bn

Nomenclature

L	Length of the artery
R	Non-stenotic radius of outer tube
K	Thermal conductivity
T	Temperature
S	Stress tensor
Q	Flow rate
Gr	Grashof number
We	Weissenberg number
$(\bar{r}, \bar{z})$	Cylindrical Coordinates
$(\bar{u}, \bar{w})$	Radial, Axial velocity
$n\ (\geq 2)$	Multiple stenosis shape parameter
$q / \frac{\partial p}{\partial z}$	Pressure gradient
a	Location of the stenosis
b	Length of the stenosis
c	Catheter radius
m	Power law index
δ	Maximum stenotic depth
g	Gravity
p	Fluid's pressure

Greek symbols

Π	Second invariant of stress tensor
η	Outer wall of artery
ϵ	Inner wall of artery
β	Dimensionless heat source or sink parameter
θ	Temperature
ζ	Maximum height attained by the clot
γ	Thermal expansion coefficient
ρ	Density
μ	Viscosity
ϕ	Nanofluid volume fraction

Subscript

nf	Nanofluid
f	Base fluid
s	Metallic nanoparticles
d	Displacement
c_p	Heat capacity

1 Introduction

A variety of cardiovascular diseases caused by stenosis or arteriosclerosis are the leading cause of mortality all over the world, which are affiliated to actions and hemodynamic circumstances of motion of blood in the artery. Stenosis is a type of uncommon constriction development caused by the build up of atherosclerotic plaques, lipids, fats, cholesterol or other unobserved substances. It arises in one or more sites in the cardiovascular system at the inner arterial wall and gives rise to crucial circulatory disorders [1]. The progression of stenosis is divided into three stages. It is mild at first stage (clogs around 5% - 15% of the blood vessel's cross-sectional passage area), then the blockage further grows to about 20% - 35% in the next phase and the flow remains laminar, but separation of flow as well as back flow happens in the vicinity of stenosis. The ultimate stage is characterized by turbulence in which the congestion surpasses 40% of the cross sectional area [2,3]. Another most frequent type of cardiovascular disease that may develop as a result of the worsening of stenosis is thrombosis, which originates from the development of thrombosis that also obstructs flow of blood in the vessels. Its growth may lead to various types of disorders and conditions, for instance, infarction, stroke, cancer and sepsis [4]. A clot in the cerebral or coronary circulation (resulting in ischemic stroke or acute myocardial infarction, respectively) is now the leading cause of worldwide illness and mortality, and the universality of both disorders is increasing, especially in developing countries [5].

In modern medicine, catheters are a common diagnostic and treatment tool. It is a fine tube that is inserted into the artery to deliver a drug or to remove the obstructions in the passage of blood. Movement of blood to crucial organs can

be improved with the use of catheters and moreover, the gas levels (oxygen and carbon dioxide) may often be measured in the bloodstream. For withdrawal of clots, a tiny needle is inserted into the blood vessel at neck, arm, leg or groin and malleable wire is stretched out into the blood vessel via the clot. In order to disintegrate, break apart and discard the clot, the catheter is guided along this wire to the location of the clot [6]. In the case of a blocked or constricted artery, a balloon can be inflated from the catheter to open up the vessel and enhance the movement of blood.

Several researchers [7–11] carried out both empirical and analytical investigation on the flow of blood via narrow stenotic arteries to diagnose the consequences of stenosis on rheological quantities like skin friction and resistance to flow. Suspension of leukocytes, thrombocytes and erythrocytes in plasma forms blood [12]. White cells (also known as Leukocytes) are relatively bigger cells $(12 - 15\mu m)$ that has an important function in preserving the immune system in our body. Red cells (commonly named as Erythrocytes) are small blood cells $(6 - 8\mu m)$ that transport oxygen-rich blood from lungs to all parts of the body and expel CO_2 from numerous sections of the body across the lungs [13]. Platelets (so called Thrombocytes) are another type of blood cell that is much smaller in size than red cells and is in-charge of forming the blood clot when it bleeds during the time of injury [14, 15].

Tiny particles suspended in liquid with at the minimum of one primary dimension less than $100nm$ are known as nanofluids. It has become the subject matter of extensive studies and biomedical implementation. Former studies reveal that nanofluids own intensified properties of thermophysics like thermal diffusivity, viscosity, thermal conductivity and coefficients of convective heat transfer in

comparison to base fluids [16–19]. Moreover, nanoparticles can be utilized in the procedure of medical treatment [20].

It is commonly agreed that at high shear rate, blood is recognised as Newtonian fluid when it moves along the bigger diameter blood vessels (diameter of blood vessel diameter $> 300\mu m$) whereas when blood moves in smaller diameter blood vessel (diameter of size $< 300\mu m$) at lower rate of shear, it acts as non-Newtonian fluid [21, 22]. Generally, the cluster of red cells is higher in the middle region when blood flows in constricted arteries while the cell depleted region is at the arterial wall. Empirical outcomes obtained from the experimental studies [23–27] disclosed that in constricted arteries, many red cells in blood are suspended along the axis of the arteries which are exemplified by non-Newtonian fluid.

As reported by Yilmaz et al. [28], Generalized Newtonian fluid expresses most characteristics of shear thinning blood. Carreau-Yasuda, Cross, Power law, Sisko, Herschel-Bulkley and Yeleswarapu are some models of non-Newtonian fluid that are frequently used to mathematically describe the rheology of blood via smaller artery diameters [29, 30]. It is known that the Carreau-Yasuda model is a generalized type of Sisko and Power law models. Many researchers revealed that Carreau fluid model is the better fitting model in exhibiting distinct features of blood dynamics since it behaves like Newtonian when the time parameter is zero and non-Newtonian fluid models otherwise. [31, 32].

Nadeem et al. [33] dealt with a nanofluid for constant flow of the Prandtl model in tapered stenotic arteries and employed homotopy perturbation method for solving the governing equations of motion. In addition, Ellahi et al. [34] also utilized the same approach in analyzing flow of blood of nanofluid along com-

posite stenosed arteries with penetrable walls. The mathematical study of Ahmed and Nadeem [35] derived exact solutions using distinct types of nanoparticles like titanium (TiO2), copper (Cu) and aluminum (Al2O3) as antimicrobials of blood movement via moderate stenosis in the lesion of arteries.

Mekheimer et al. [36, 37] studied the impacts of copper nanoparticles on the motion of blood along a stenotic artery when magnetic field presents. The consequences of dilatation and constriction were taken into account in the work of [38] by investigating the unusual nature of the wall sections with variable nanofluid viscosity in the motion of blood via artery and assuming blood as a viscous fluid. Thenceforth, Akbar [39] conducted an analysis of pure water and copper-blood flow model and subsequently obtained precise solutions for nature of blood movement for various types of tapered stenotic arteries.

Nadeem et al. [40] studied the impact of metallic nanoparticles on blood motion via catheterized tapered flexible intersecting stenosed artery with magnetic field varying with radial direction. Elnaqeeb et al. [6] examined copper nanoparticles for motion of blood along a catheterized mild stenotic artery with a clot. Recently, motion of blood along an artery with diversified stenoses and a thrombus was explicated by Zidan et al. [41]. They implemented entropy analysis for a comprehensive study of irreversibility. Due to the numerous applications of nanoparticles in the field of biomedicine, several researchers [42–50] considered the flow of fluid with the suspension of nanoparticles to investigate their effects under various rheological states.

This contemporary work deals with metallic nanoparticles in flow of blood along a catheterized mild stenotic artery with thrombosis, modelling blood as non-Newtonian Carreau fluid. The governing equations are solved by the method of

perturbation and the expressions of velocity, pressure gradient, temperature, skin friction and resistance to flow are acquired both analytically and numerically by the extensive use of MATLAB and MATHEMATICA softwares. The influences of Weissenberg number, axial displacement of the blood clot, maximum stenotic depth, stenosis shape parameter on the aforementioned flow quantification are displayed graphically and tabularly. Clinical applications of the study with the effects of several geometrical and physiological parameters on blood rheology are also analyzed in this study. The schematic diagram shown in Figure 1 describes the organization of the present mathematical model.

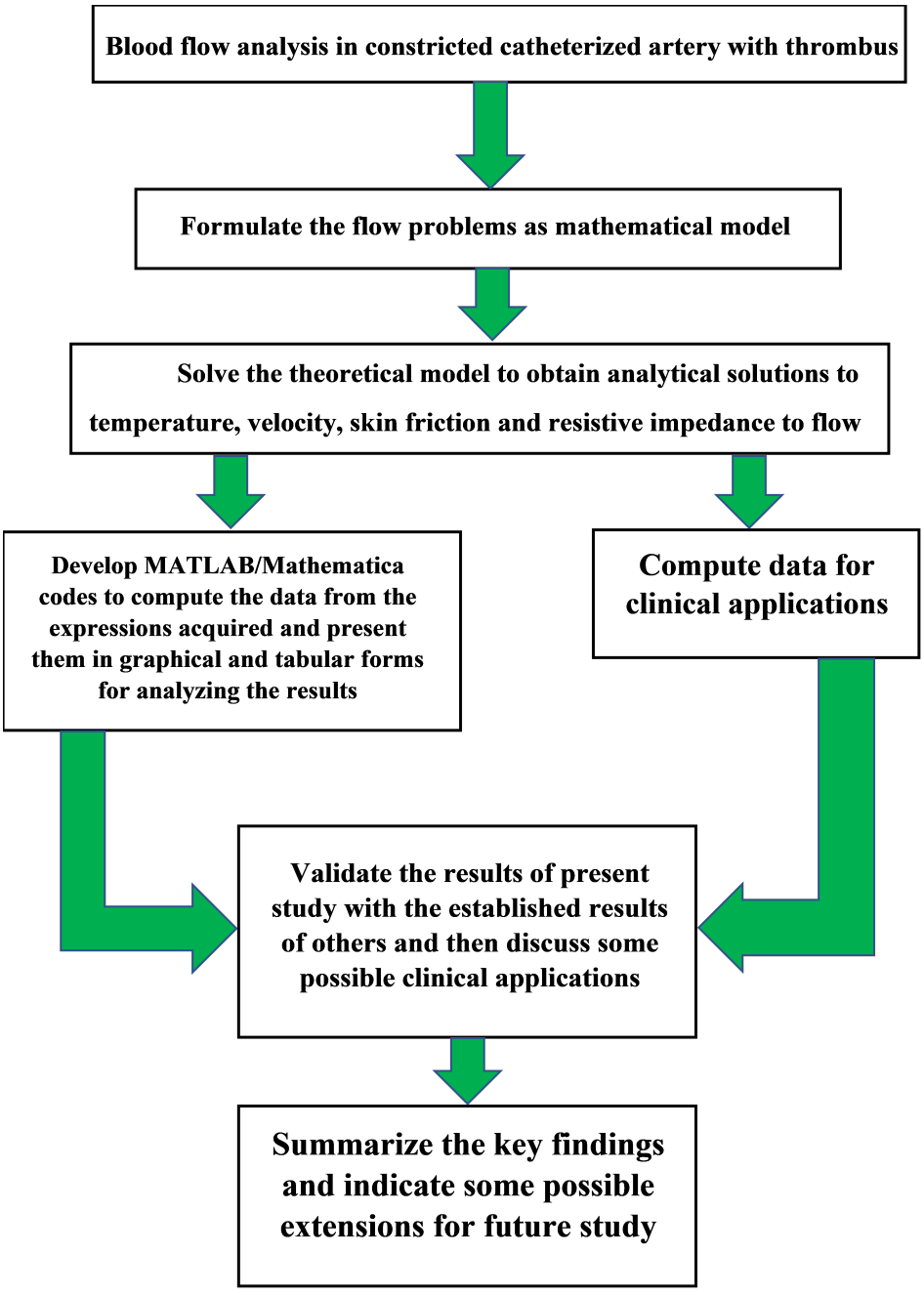

Fig. 1. Schematic configuration of the fluid flow system under study.

2 Mathematical Formulation

Let us examine the mathematical model for the incompressible, steady flow of copper nanoparticles blood along a circular artery of length L which is assumed to be comprised of two coaxial tubes; the outer tube that is axisymmetric with moderate stenosis and the inner tube which has a thrombosis where the catheter is introduced coaxially, considering blood as non-Newtonian Carreau fluid. Figure 2 depicts the geometry of segment of artery under investigation. The inner and the outer walls are denoted by $\epsilon(z)$ and $\eta(z)$, respectively, and can be mathematically represented as below:

$$\begin{aligned} \bar{\epsilon}(\bar{z}) &= \bar{R}[c + \zeta e^{-\pi^2(\bar{z}-z_d-0.5)^2}], && \bar{a} \leq \bar{z} \leq \bar{a} + \bar{b} \\ &= c\bar{R}, && \text{otherwise} \end{aligned} \tag{1}$$

$$\begin{aligned} \bar{\eta}(\bar{z}) &= \bar{R}\left[1 - \bar{\kappa}\left(\bar{b}^{n-1}(\bar{z} - \bar{a}) - (\bar{z} - \bar{a})^n\right)\right], && \bar{a} \leq \bar{z} \leq \bar{a} + \bar{b} \\ &= \bar{R}, && \text{otherwise} \end{aligned} \tag{2}$$

where ζ is the utmost height attained by the clot at $\bar{z} = z_d + 0.5$, $c\bar{R}$ is the inner tube's radius in which $c \ll 1$, and z_d is the clot's axial displacement, $\bar{R}$ is the artery's radius in the non-stenotic region, $\bar{b}$ is the length of the stenosis, $n \geq 2$ is the shape parameter of stenosis, $\bar{a}$ is the site of stenosis and $\bar{\kappa}$ is delineated by

$$\bar{\kappa} = \frac{\bar{\delta}^*}{\bar{R}\bar{b}^n} \frac{n^{\frac{n}{n-1}}}{n-1} \tag{3}$$

where $\bar{\delta}^*$ is the utmost stenotic depth placed at $\bar{z} = \bar{a} + \frac{\bar{b}}{n^{\frac{1}{n-1}}}$.

By assuming the flow of blood along the artery is asymmetric, the difference in

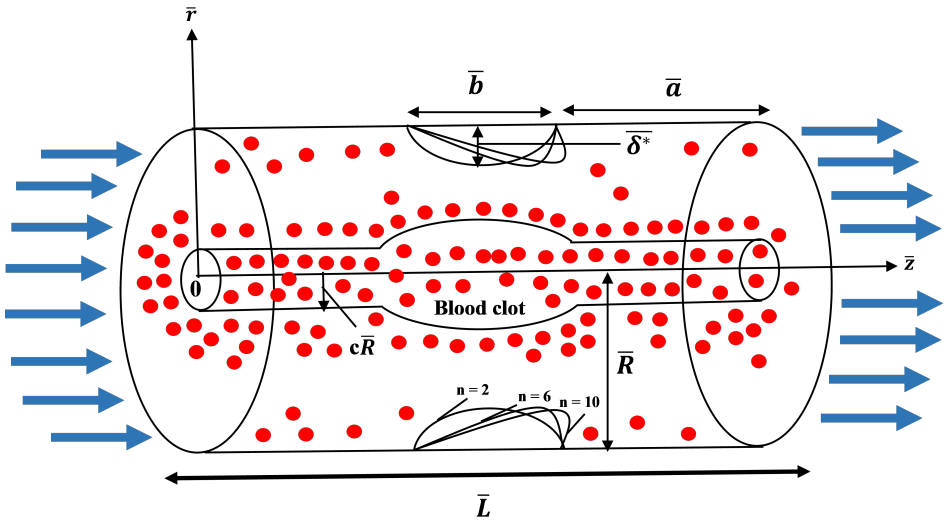

Fig. 2. Geometry of a mild stenotic catheterized artery with thrombus

the characteristic of blood motion is not dependent on the azimuthal angle. Thus, the governing equations of the steady flow of an incompressible viscous nanofluid along a catheterized mild stenotic artery with thrombosis in the presence of gravity as a body force, are

$$\frac{\partial \bar{u}}{\partial \bar{r}} + \frac{\bar{u}}{\bar{r}} + \frac{\partial \bar{w}}{\partial \bar{z}} = 0 \tag{4}$$

$$\rho_{nf}\left(\bar{u}\frac{\partial \bar{w}}{\partial \bar{r}} + \bar{w}\frac{\partial \bar{w}}{\partial \bar{z}}\right) = -\frac{\partial \bar{p}}{\partial \bar{z}} + \frac{1}{\bar{r}}\frac{\partial}{\partial \bar{r}}\left(\bar{r}\bar{S}_{\bar{r}\bar{z}}\right) + \frac{\partial}{\partial \bar{z}}\left(\bar{S}_{\bar{z}\bar{z}}\right) + g(\rho\gamma)_{nf}\left(\bar{T} - \bar{T}_0\right) \tag{5}$$

$$\rho_{nf}\left(\bar{u}\frac{\partial \bar{u}}{\partial \bar{r}} + \bar{w}\frac{\partial \bar{u}}{\partial \bar{z}}\right) = -\frac{\partial \bar{p}}{\partial \bar{r}} - \left(\frac{1}{\bar{r}}\frac{\partial}{\partial \bar{r}}\left(\bar{r}\bar{S}_{\bar{r}\bar{r}}\right) + \frac{\partial}{\partial \bar{z}}\left(\bar{S}_{\bar{r}\bar{z}}\right)\right) \tag{6}$$

$$\bar{u}\frac{\partial \bar{T}}{\partial \bar{r}} + \bar{w}\frac{\partial \bar{T}}{\partial \bar{z}} = \frac{K_{nf}}{(\rho c_p)_{nf}}\left(\frac{\partial^2 \bar{T}}{\partial \bar{r}^2} + \frac{1}{\bar{r}}\frac{\partial \bar{T}}{\partial \bar{r}} + \frac{\partial^2 \bar{T}}{\partial \bar{z}^2}\right) + \frac{Q_0}{(\rho c_p)_{nf}} \tag{7}$$

In Eqs. (4) - (7), $\bar{z}$ and $\bar{r}$ axes are taken as axial and radial direction, respectively, u and w are the components of radial and axial velocity, accordingly, g is the gravity, p is the fluid pressure and Q_0 is the constant heat generation or absorption. For the suggested model of nanofluid, γ_{nf} is the thermal expansion coefficient of nanofluid, $(\rho c_p)_{nf}$ is the heat capacitance of nanofluid, ρ_{nf} is the nanofluid density, K_{nf} is the thermal conductivity of nanofluid and μ_{nf} is the nanofluid viscosity. The heat transfer is also considered by assuming T_0 and T_1 as the temperatures at the arterial wall and catheter, accordingly.

Since the heat transfer is also considered in the study, the last term $g(\rho\gamma)_{nf}(T - T_0)$ in Eq. 5 corresponds to the natural convective heat transfer in blood flow which occurs in radial direction due to the presence of metallic nanoparticles in blood. Thus, the effect of gravitational force is inherent in the blood flow with heat transfer and this acts in the radial direction.

The constitutive equation of non-Newtonian Carreau fluid which defines the nonlinear relation between the shear stress and rate of shear, is given below:

$$\frac{(\bar{\mu} - \bar{\mu}_\infty)}{(\bar{\mu}_0 - \bar{\mu}_\infty)} = \left[1 + (\bar{\Gamma}\dot{\bar{\gamma}})^2\right]^{\left(\frac{m-1}{2}\right)} \tag{8}$$

$$\bar{S}_{ij} = \bar{\mu}_0\left[1 + \frac{(m-1)}{2}(\bar{\Gamma}\dot{\bar{\gamma}})^2\right]\dot{\bar{\gamma}}_{ij} \tag{9}$$

in which $\bar{S}_{ij}$ is the extra stress tensor, $\bar{\mu}_\infty$ is the finiteless rate of shear viscosity, $\bar{\mu}_0$ is the zero rate of shear viscosity, Γ is the time dependent constant, m is the

power law index and $\dot{\gamma}$ is the rate of shear which is depicted as

$$\bar{\dot{\gamma}} = \sqrt{\frac{1}{2}\sum_i \sum_j \bar{\dot{\gamma}}_{ij}\bar{\dot{\gamma}}_{ji}} = \sqrt{\frac{1}{2}\Pi} \tag{10}$$

Here, Π is the second invariant strain tensor.

The dimensional form of boundary conditions pertaining to the assumed blood flow are

$$\begin{aligned} &\bar{T} = \bar{T}_1 \text{ at } \bar{r} = \bar{\epsilon}(\bar{z}) \text{ and } \bar{T} = \bar{T}_0 \text{ at } \bar{r} = \bar{\eta}(\bar{z}) \\ &\bar{w} = \ 0 \text{ at } \bar{r} = \bar{\epsilon}(\bar{z}) \text{ and } \bar{w} = 0 \text{ at } \bar{r} = \bar{\eta}(\bar{z}) \end{aligned} \tag{11}$$

The nanofluid's thermo physical properties are defined by the following equations [51]:

$$\begin{aligned} &\alpha_{nf} = \frac{K_{nf}}{(\rho c_p)_{nf}}, \\ &\rho_{nf} = (1-\phi)\,\rho_f + \phi\rho_s, \\ &(\rho c_p)_{nf} = (1-\phi)\,(\rho c_p)_f + \phi(\rho c_p)_s, \\ &(\rho\gamma)_{nf} = (1-\phi)\,(\rho\gamma)_f + \phi(\rho\gamma)_s, \\ &\mu_{nf} = \frac{\mu_f}{(1-\phi)^{2.5}}, \\ &\frac{K_{nf}}{K_f} = \frac{\big(K_s+2K_f\big)-2\phi\big(K_f-K_s\big)}{\big(K_s+2K_f\big)+\phi\big(K_f-K_s\big)}, \end{aligned} \tag{12}$$

where $K_f, \rho_f, (\rho c_p)_f, \mu_f$ and γ_f are thermal conductivity, density, heat capacitance, viscosity and the base fluid's thermal expansion coefficient, accordingly, while $K_s, \rho_s, (\rho c_p)_s, \mu_s$ and γ_s are thermal conductivity, density, heat capacitance, viscosity and thermal expansion coefficient of the metallic nanoparticles, respectively and ϕ is volume fraction of the nanofluid.

The dimensionless quantities are demonstrated as below:

$$r = \frac{\bar{r}}{\bar{R}},\ z = \frac{\bar{z}}{\bar{b}},\ w = \frac{\bar{w}}{\bar{u}_0},\ u = \frac{L\bar{u}}{\bar{u}_0\bar{\delta}^*},\ p = \frac{\bar{R}^2\bar{p}}{4\bar{u}_0\bar{b}\mu_f},$$

$$\beta = \frac{\bar{R}^2\bar{a}}{4\bar{u}_0\mu_f},\ Gr = \frac{g\nu_f\rho_f\bar{R}^2\bar{T}_0}{\bar{u}_0\mu_f},\ \theta = \frac{\bar{T}-\bar{T}_0}{\bar{T}_1-\bar{T}_0}, \tag{13}$$

$$Q = \frac{\bar{Q}}{\bar{R}^2\bar{u}_0},\ \ We = \frac{\Gamma\bar{u}_0}{\bar{R}}$$

where $\bar{u}_0$ is the averaged velocity of the channel segment of width R, β is the dimensionless parameter of heat source or sink of the fluid, θ is the temperature, Q is the flow rate, Gr is the Grashof number and We is the Weissenberg number. Considering the flow as slow flow (low Reynolds number) and then utilizing the dimensionless variables, we obtain the following conceptual approximation to the assumed fluid flow model:

$$\frac{Rn^{\frac{1}{n-1}}}{b} \sim O(1) \tag{14}$$

$$\delta = \frac{\delta^*}{R} \ll 1 \tag{15}$$

By utilizing the dimensionless variables in the momentum equations (5)-(7), one can attain the reduced form of governing equations as follows:

$$\frac{\partial p}{\partial r} = 0 \tag{16}$$

$$-4\frac{\partial p}{\partial z} - \frac{1}{r}\frac{\partial}{\partial r}\left[r\left\{\left(\frac{\partial w}{\partial r}\right) + We^2\left(\frac{m-1}{2}\right)\left(\frac{\partial w}{\partial r}\right)^3\right\}\right] + \frac{Gr\theta}{(\rho\gamma)_f} = 0 \tag{17}$$

$$\frac{\partial^2\theta}{\partial r^2} + \frac{1}{r}\frac{\partial\theta}{\partial r} + \beta\frac{K_f}{K_{nf}} = 0 \tag{18}$$

The boundary conditions in (11) reduce to the dimensionless form as below:

$$\begin{aligned} &\theta = 0 \text{ at } r = \eta(z) \text{ and } \theta = 1 \text{ at } r = \epsilon(z) \\ &w = 0 \text{ at } r = \eta(z) \text{ and } w = 0 \text{ at } r = \epsilon(z) \end{aligned} \tag{19}$$

where $\epsilon(z)$ and $\eta(z)$ in non-dimensional form become

$$\begin{aligned} \varepsilon(z) &= c + \zeta e^{-\pi^2 b^2\left(z - \frac{z_d + 0.5}{b}\right)^2} && h \le z \le h+1, \\ &= c && \text{otherwise} \end{aligned} \tag{20}$$

$$\begin{aligned} \eta(z) &= 1 - \kappa^* \left[b^{n-1}(z-a) - (z-a)^n\right] && h \le z \le h+1, \\ &= 1 && \text{otherwise} \end{aligned} \tag{21}$$

and

where $h = \frac{a}{b}$, $\kappa^* = \delta\frac{n^{\frac{n}{n-1}}}{n-1}$ and $\delta = \frac{\delta^*}{R}$.

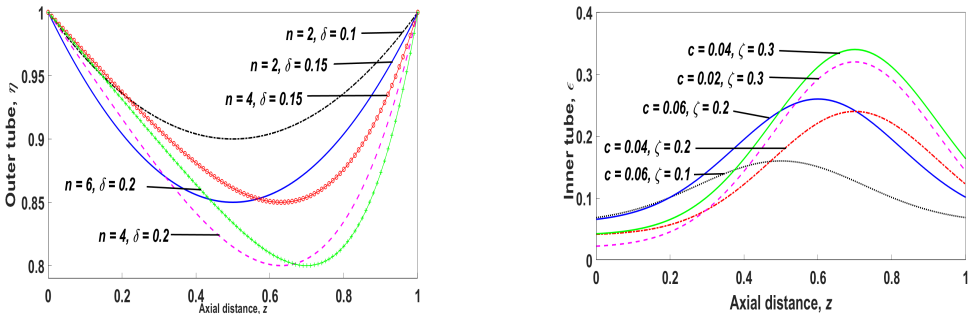

(a) Outer tube **(b)** Inner tube

Fig. 3. Geometry of the outer tube η and inner tube ϵ with $R = 1, a = 0$ and $b = 1$ and for **(a)** various n and δ values and **(b)** various c and ζ values.

Figs. 3a and 3b represent the geometry of arterial segment with stenosis and thrombosis, respectively. Since stenosis occurs at the outer tube, the stenosis has

peak in the downward direction and the blood clot (thrombosis) has developed at the inner tube, the blood clot has peak in the upward direction.

3 Solution Method

Solving Eq. (18) by employing the corresponding boundary conditions, one can easily obtain the general solution of temperature as below:

$$\theta = -\frac{\beta}{4}\frac{K_f}{K_{nf}}\left(r^2-\eta^2\right)+\frac{\ln\left(\frac{r}{\eta}\right)}{\ln\left(\frac{\varepsilon}{\eta}\right)}\left(1-\frac{\beta}{4}\frac{K_f}{K_{nf}}\left(\eta^2-\varepsilon^2\right)\right) \tag{22}$$

3.1 Perturbation solution

Let us denote the pressure gradient $\frac{dp}{dz}$ by q. In order to attain the perturbation solution of axial velocity, w, we expand w corresponding to the parameter of perturbation We^2 (Weissenberg number) as given below:

$$w = w_0 + We^2 w_1 + O\big(We^2\big)^2 \tag{23}$$

On using Eq. (22) in Eq.(17) and then employing the series of perturbation expansion (23) in the resulting equation and solving the decomposed system of differential equations through the utilization of the boundary conditions (19), one can acquire the solution to the axial velocity analytically as presented below:

$$w = q\left(\eta^2-r^2\right)+\frac{Gr}{(\rho\gamma)_f}f\left(r\right)+\frac{\ln\left(\frac{r}{\eta}\right)}{\ln\left(\frac{\varepsilon}{\eta}\right)}\left[q\left(\varepsilon^2-\eta^2\right)+\frac{Gr}{(\rho\gamma)_f}f\left(\varepsilon\right)\right]+We^2[w_1] \tag{24}$$

where $f(r)$, $f(\epsilon)$ and w_1 are depicted as

$$f(r) = -\frac{\beta}{4}\frac{K_f}{K_{nf}}\left(\frac{r^4}{16} - \frac{\eta^2 r^2}{4} + \frac{3\eta^4}{16}\right) + \frac{\left(r^2 \ln\left(\frac{r}{\eta}\right) - r^2 + \eta^2\right)}{4\ln\left(\frac{\varepsilon}{\eta}\right)}\left\{1 - \frac{\beta}{4}\frac{K_f}{K_{nf}}\left(\eta^2 - \varepsilon^2\right)\right\} \tag{25}$$

$$f(\varepsilon) = -\frac{\beta}{4}\frac{K_f}{K_{nf}}\left(\frac{\eta^2\varepsilon^2}{4} - \frac{\varepsilon^4}{16} - \frac{3\eta^4}{16}\right) + \frac{\left(\varepsilon^2 - \eta^2 - \varepsilon^2 \ln\left(\frac{\varepsilon}{\eta}\right)\right)}{4\ln\left(\frac{\varepsilon}{\eta}\right)}\left\{1 - \frac{\beta}{4}\frac{K_f}{K_{nf}}\left(\eta^2 - \varepsilon^2\right)\right\} \tag{26}$$

$$w_1 = \left(\tfrac{m-1}{2}\right)\left[\left(2\varepsilon^4 - 2r^4\right)q^3 + \tfrac{\left(6\varepsilon^2 - 6r^2\right)}{\ln\left(\frac{\varepsilon}{\eta}\right)}\left(q^3\left\{\varepsilon^2 - \eta^2\right\}\right) - \tfrac{q^3\left\{\varepsilon^2-\eta^2\right\}^3}{\left\{2r^2-2\varepsilon^2\right\}\left(\ln\left(\frac{\varepsilon}{\eta}\right)\right)^3}\right]$$

$$+\tfrac{\ln\left(\frac{r}{\varepsilon}\right)}{\ln\left(\frac{\eta}{\varepsilon}\right)}\left[\left(\tfrac{m-1}{2}\right)\left[\left(2\eta^4 - 2\varepsilon^4\right)q^3 + \tfrac{\left(6\eta^2 - 6\varepsilon^2\right)}{\ln\left(\frac{\varepsilon}{\eta}\right)}\left(q^3\left\{\varepsilon^2 - \eta^2\right\}\right) - \tfrac{q^3\left\{\varepsilon^2-\eta^2\right\}^3}{\left\{2\varepsilon^2-2\eta^2\right\}\left(\ln\left(\frac{\varepsilon}{\eta}\right)\right)^3}\right]\right] \tag{27}$$

Now, one can obtain the expression for stream function ψ by utilizing the equation $w = \frac{1}{r}\frac{\partial\psi}{\partial r}$ and the condition $\psi = 0$ at $r = \epsilon$. Hence, the corresponding stream function can be obtained in the following form

$$\psi = q\left(\tfrac{\eta^2 r^2}{2} + \tfrac{1}{4}\left\{\varepsilon^4 - r^4\right\} - \tfrac{\eta^2\varepsilon^2}{2}\right) + \tfrac{Gr}{(\rho\gamma)_f}\psi_a$$

$$+\tfrac{2r^2\ln\left(\frac{r}{\eta}\right) - r^2 + 2\varepsilon^2\ln\left(\frac{\varepsilon}{\eta}\right) - \varepsilon^2}{4\ln\left(\frac{\varepsilon}{\eta}\right)}\left[q\left(\varepsilon^2 - \eta^2\right) + \tfrac{Gr}{(\rho\gamma)_f}\psi_b\right] \tag{28}$$

$$-We^2\left[\left(\tfrac{m-1}{2}\right)\psi_c + \tfrac{2r^2\ln\left(\frac{r}{\varepsilon}\right) - r^2 - \varepsilon^2}{4\ln\left(\frac{\eta}{\varepsilon}\right)}\left[\left(\tfrac{m-1}{2}\right)\psi_d\right]\right]$$

where

$$\psi_a = -\tfrac{\beta}{4}\tfrac{K_f}{K_{nf}}\left\{\tfrac{r^6-\varepsilon^6}{96} + \tfrac{3\eta^4}{32}\left(r^2-\varepsilon^2\right) + \tfrac{\eta^2}{16}\left(\varepsilon^4-r^4\right)\right\} + \left\{1 - \tfrac{\beta}{4}\tfrac{K_f}{K_{nf}}\left(\eta^2-\varepsilon^2\right)\right\}\tfrac{\left\{\frac{r^4}{4}\ln\left(\frac{r}{\eta}\right)+\frac{5}{16}\left(\varepsilon^4-r^4\right)+\frac{\eta^2}{2}\left(r^2-\varepsilon^2\right)-\frac{\varepsilon^4}{4}\ln\left(\frac{\varepsilon}{\eta}\right)\right\}}{4\ln\left(\frac{\varepsilon}{\eta}\right)} \tag{29}$$

$$\psi_b = -\frac{\beta}{4}\frac{K_f}{K_{nf}}\left\{\frac{4\eta^2\varepsilon^2-3\eta^4-\varepsilon^4}{16}\right\}+\frac{\left\{\varepsilon^2-\eta^2-\varepsilon^2\ln\left(\frac{\varepsilon}{\eta}\right)\right\}}{4\ln\left(\frac{\varepsilon}{\eta}\right)}\left\{1-\frac{\beta}{4}\frac{K_f}{K_{nf}}\left(\eta^2-\varepsilon^2\right)\right\} \tag{30}$$

$$\psi_c = q^3\left[\begin{array}{l}\varepsilon^4 r^2 - \frac{r^6}{3} - \frac{2}{3}\varepsilon^6 + \left(\varepsilon^2-\eta^2\right)\times \\ \left\{\frac{3\varepsilon^2 r^2 - \frac{3}{2}\left(r^4+\varepsilon^4\right)}{\ln\left(\frac{\varepsilon}{\eta}\right)} - \left(\varepsilon^2-\eta^2\right)^2\left\{\frac{\ln\left(2r^2-2\varepsilon^2\right)}{4\left\{\ln\left(\frac{\varepsilon}{\eta}\right)\right\}^3}\right\}\right\}\end{array}\right] \tag{31}$$

$$\psi_d = q^3\left[\left(2\eta^4-2\varepsilon^4\right)+\left(\varepsilon^2-\eta^2\right)\left\{\frac{6\eta^2-6\varepsilon^2}{\ln\left(\frac{\varepsilon}{\eta}\right)} - \frac{\left(\varepsilon^2-\eta^2\right)^2}{\left(2\varepsilon^2-2\eta^2\right)\left(\ln\left\{\frac{\varepsilon}{\eta}\right\}\right)^3}\right\}\right] \tag{32}$$

The flow rate Q is defined by

$$Q = \int_{\varepsilon}^{\eta} rwdr \tag{33}$$

The ultimate expression of Q is obtained as below:

$$Q = q\left(\frac{\eta^4}{4} - \frac{\eta^2\varepsilon^2}{2} + \frac{\varepsilon^4}{4}\right) + \frac{Gr}{(\rho\gamma)_f}Q_a + \frac{\varepsilon^2-\eta^2-2\varepsilon^2\ln\left(\frac{\varepsilon}{\eta}\right)}{4\ln\left(\frac{\varepsilon}{\eta}\right)}\left[q\left(\varepsilon^2-\eta^2\right) + \frac{Gr}{(\rho\gamma)_f}Q_b\right]$$

$$+We^2\left[\left(\frac{m-1}{2}\right)Q_c + \frac{2\eta^2\ln\left(\frac{\eta}{\varepsilon}\right)-\eta^2+\varepsilon^2}{4\ln\left(\frac{\eta}{\varepsilon}\right)}\left\{\frac{m-1}{2}Q_d\right\}\right] \tag{34}$$

where

$$Q_a = -\frac{\beta}{4}\frac{K_f}{K_{nf}}\left(\frac{\eta^6}{24} - \frac{\varepsilon^6}{96} + \frac{\eta^2\varepsilon^2}{16} - \frac{3\eta^4\varepsilon^2}{32}\right) + \frac{\left\{\frac{3\eta^4}{8} - \frac{\varepsilon^4}{4}\ln\left(\frac{\varepsilon}{\eta}\right) + \frac{\varepsilon^4}{8} - \frac{\eta^2\varepsilon^2}{2}\right\}}{4\ln\left(\frac{\varepsilon}{\eta}\right)} \times \left\{1 - \frac{\beta}{4}\frac{K_f}{K_{nf}}\left(\eta^2-\varepsilon^2\right)\right\} \tag{35}$$

$$Q_b = -\frac{\beta}{4}\frac{K_f}{K_{nf}}\left(-\frac{3\eta^4}{16} - \frac{\varepsilon^4}{16} + \frac{\eta^2\varepsilon^2}{4}\right) + \frac{\left\{\varepsilon^2-\eta^2-\varepsilon^2\ln\left(\frac{\varepsilon}{\eta}\right)\right\}}{4\ln\left(\frac{\varepsilon}{\eta}\right)}\left\{1 - \frac{\beta}{4}\frac{K_f}{K_{nf}}\left(\eta^2-\varepsilon^2\right)\right\} \tag{36}$$

$$Q_c = q^3\left[\varepsilon^4\eta^2 - \frac{\eta^6}{3} - \frac{2\varepsilon^6}{3} + \left(\varepsilon^2-\eta^2\right)\left\{\frac{3\varepsilon^2\eta^2 - \frac{3}{2}\left(\eta^4+\varepsilon^4\right)}{\ln\left(\frac{\varepsilon}{\eta}\right)} - \frac{\left(\varepsilon^2-\eta^2\right)^2\ln\left(2\eta^2-2\varepsilon^2\right)}{4\left\{\ln\left(\frac{\varepsilon}{\eta}\right)\right\}^3}\right\}\right] \tag{37}$$

$$Q_d = q^3\left[\left(2\eta^4-2\varepsilon^4\right) + \left(\varepsilon^2-\eta^2\right)\left\{\frac{6\eta^2-6\varepsilon^2}{\ln\left(\frac{\varepsilon}{\eta}\right)} - \frac{\left(\varepsilon^2-\eta^2\right)^2}{\left(2\varepsilon^2-2\eta^2\right)\left\{\ln\left(\frac{\varepsilon}{\eta}\right)\right\}^3}\right\}\right] \tag{38}$$

By presuming total volumetric flow rate, Q as constant, one can calculate the pressure gradient, q for distinct parameter values involved in the present study.

The wall shear stress can be derived as

$$S_{rz} = 2\eta q - \frac{Gr}{(\rho\gamma)_f} S_{rz1} - \frac{1}{\eta \ln\left(\frac{\varepsilon}{\eta}\right)} \left[q\left(\varepsilon^2 - \eta^2\right) + \frac{Gr}{(\rho\gamma)_f} S_{rz2} \right] \\ -We^2 \left[\left(\frac{m-1}{2}\right) S_{rz3} + \frac{1}{\eta \ln\left(\frac{\eta}{\varepsilon}\right)} \left\{ \left(\frac{m-1}{2}\right) S_{rz4} \right\} \right] \tag{39}$$

where

$$S_{rz1} = -\frac{\beta}{4}\frac{K_f}{K_{nf}} \left(-\frac{\eta^3}{4} \right) - \frac{\eta}{4 \ln\left(\frac{\varepsilon}{\eta}\right)} \left\{ 1 - \frac{\beta}{4}\frac{K_f}{K_{nf}} \left(\eta^2 - \varepsilon^2\right) \right\} \tag{40}$$

$$S_{rz2} = -\frac{\beta}{4}\frac{K_f}{K_{nf}} \left(-\frac{3\eta^4}{16} - \frac{\varepsilon^4}{16} + \frac{\eta^2\varepsilon^2}{4} \right) + \frac{\left(\varepsilon^2 - \eta^2 - \varepsilon^2 \ln\left(\frac{\varepsilon}{\eta}\right)\right)}{4 \ln\left(\frac{\varepsilon}{\eta}\right)} \left\{ 1 - \frac{\beta}{4}\frac{K_f}{K_{nf}} \left(\eta^2 - \varepsilon^2\right) \right\} \tag{41}$$

$$S_{rz3} = -8\eta^3 q^3 + \frac{(-12\eta)}{\ln\left(\frac{\varepsilon}{\eta}\right)} \left(q^3 \left(\varepsilon^2 - \eta^2\right) \right) + \frac{4q^3(\varepsilon^2 - \eta^2)^3}{\eta^3 \left(\ln\left(\frac{\varepsilon}{\eta}\right) \right)^3} \tag{42}$$

$$S_{rz4} = \left(2\eta^4 - 2\varepsilon^4\right) q^3 + \frac{(6\eta^2 - 6\varepsilon^2)}{\ln\left(\frac{\varepsilon}{\eta}\right)} q^3 \left(\varepsilon^2 - \eta^2\right) - \frac{q^3(\varepsilon^2 - \eta^2)^3}{(2\varepsilon^2 - 2\eta^2) \left(\ln\left(\frac{\varepsilon}{\eta}\right) \right)^3} \tag{43}$$

The resistive impedance can be obtained as

$$\lambda = \frac{\Delta p}{Q} \tag{44}$$

In order to get the resistance to flow, numerical integration is performed through the use of MATLAB software. For several parameter values contained in this

study, numerical values of λ can be calculated and are presented in the next section through graphical results as well as physiological data.

The solutions obtained so far to various flow quantities of Carreau fluid model reduce to those of Newtonian fluid when $We = 0$ or $m = 1$ and are in good agreement with the corresponding solutions obtained for Newtonian fluid by Elnaqeeb et al. [6].

Table 1: Thermophysical properties of base fluid (blood) and copper nano particles.

Physical quantities	**Blood**	**Copper (Cu)**
$c_p(\mathrm{J/kgK})$	3594	385
$\rho(\mathrm{kg/m^3})$	1063	8933
$K(\mathrm{W/mK})$	0.492	400
$\gamma\ \mathrm{x10^{-5}(K^{-1})}$	0.18	1.67

4 Numerical Simulation of Results

MATLAB and MATHEMATICA softwares are extensively used to numerically evaluate the analytical solutions obtained for temperature, pressure gradient, velocity distribution, skin friction and resistance to flow, to generate data for graphical and tabular representation of results and also to present some data for the clinical applications of the current study. These graphs interpret the results for different kinds physiological states such as stenosis in arteries with thrombus in the presence of catheter ($c \neq 0$) and in the absence of catheter ($c = 0$). The thermophysical quantities for density ρ, specific heat capacity c_p, thermal conductivity K and coefficient of thermal expansion γ for both copper nano particles and blood are extracted from [52, 53] and are recorded in Table 1.

The range of values of parameters implemented in the computation of data for graphical results and tabulated data are presented below:

Table 2: Range of values of parameters

Parameters	**Symbol**	**Range**
Stenosis length	L	1
Radius of the unconstricted artery	$\bar{R}$	1
Length of stenosis	b	1
Power law index	m	2
Shape parameter of stenosis	n	2 - 11
Radius of catheter	c	0 - 0.6
Axial displacement of the clot	z_d	0 - 0.6
Utmost stenotic depth	δ	0.05 - 0.4
Utmost depth of blood clot	ζ	0.05 - 0.2
Flow rate	Q	0.03 - 0.95
Dimensionless heat source or sink parameter	β	0.1 - 0.5
Grashof number	Gr	2 - 5
Weissenberg number	We	0.05 - 0.7

4.1 Temperature distribution

Fig. 4a presents the variation of temperature profile radially for various values of stenosis shape parameter n. As the stenosis shape develops, the temperature decreases due to the decreased blood motion in the artery. This behaviour is also visualized in Fig. 4b when the stenosis depth increases and the reverse trend in temperature variation is noted in Fig. 4c when the depth of the blood clot increases (due to the reduced supply of oxygen in the blood stream). In all the three cases, one can note that in the presence of a catheter, the temperature values are always higher.

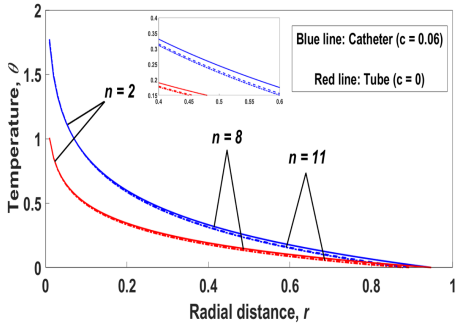

(a) Different n

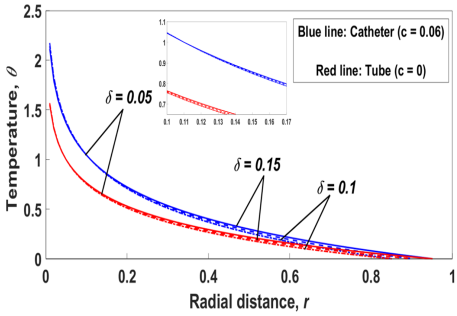

(b) Different δ

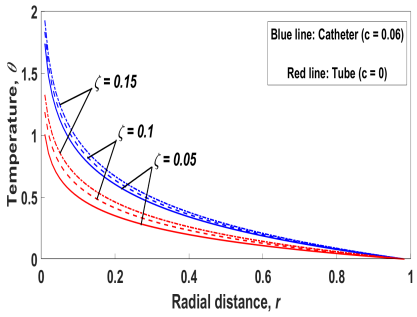

(c) Different ζ

Fig. 4. Temperature with radial distance for **(a)** several n values, **(b)** several δ values and **(c)** several ζ values with $z = 0.9, b = 1, R = 1, a = 0, \beta = 0.2$ and $z_d = 0$.

4.2 Pressure gradient

Figs. 5a - 5e shows the axial variation of pressure gradient for distinct values of parameters (a) n, (b) ζ, (c) δ, (d) z_d and (e) Q with $R = 1, b = 1, a = 0, m = 2, We = 0.1, Gr = 5$ and $\beta = 0.5$. In Fig. 5a, pressure gradient seems to rise when the stenosis shape parameter n decreases owing to the existence of both the stenosis and the blood clot. As the blood clotting thickens, the opposite trend in pressure gradient is recognized in Fig. 5b, because as the blood flows through the narrow artery, it demands more pressure to navigate the blood to move along the downstream.

Fig. 5c illustrates the variation of pressure gradient axially for several values of stenosis depth δ. As in the case of blood clot, the thickening of the stenosis results in the increase of pressure gradient. The difference of axial displacement of the thrombus are portrayed in Fig. 5d with values 0.1, 0.3 and 0.5. It can be observed that when z_d increases from 0.1 to 0.3, the pressure gradient reduces significantly with the existence of catheter and considerably when catheter is in use. It is also visible that the skewness in pressure gradient are more towards the right side as z_d rises. In Fig. 5e, variation of flow rate Q for three distinct values are plotted against axial distance, z and it is spotted that as the flow rate surges from 0.75 to 0.85 then to 0.95, the pressure gradient also increase marginally.

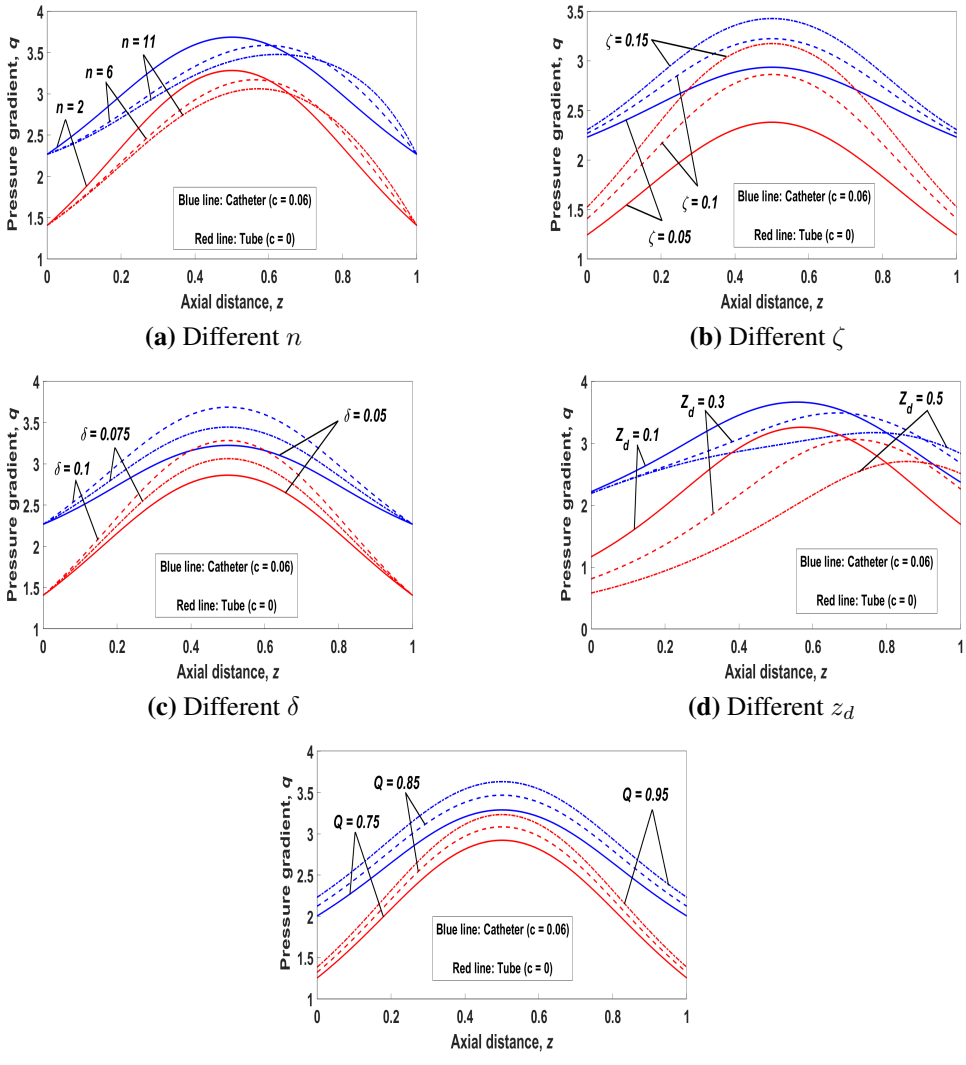

(a) Different n **(b)** Different ζ

(c) Different δ **(d)** Different z_d

(e) Different Q

Fig. 5. Pressure gradient with axial distance for **(a)** several n values, **(b)** several ζ values, **(c)** several δ values, **(d)** several z_d values and **(e)** several Q values with $R = 1, b = 1, a = 0, m = 2, We = 0.1, Gr = 5$ and $\beta = 0.5$.

4.3 Velocity distribution

Figs. 6a - 6e illustrates the variation of velocity distribution radially for several values of the parameters (a) n, (b) ζ, (c) z_d, (d) Q and (e) We with $R = 1, b = 1, a = 0, m = 2$ and $Gr = 5$. Fig. 6a depicts that when the shape parameter of stenosis n grows and in the absence of catheter, the fluid velocity descends in the range of r from 0 to 0.5 and it begins to increase in the range of r from 0.5 to 0.84. The reverse trend is noticed in the existence of catheter when r is around 0.1 to 0.2. The axial displacement of the clot plays a significant role for this abnormal behavior.

Fig. 6b delineates the velocity profile for distinct values of ζ. In both tubes (with and without catheter), the thickness of the thrombus (along with 5% stenosis) results in the decrease of the velocity when r varies in the range 0 - 0.3. It then increases slightly when r rises from 0.3 to 0.94. From Fig. 6c, one can observe that as the clot displaces further, velocity raises. When the flow rate rises, the fluid's velocity increases which is depicted in Fig. 6d. This is due to the narrowing of the artery in the existence of both stenosis and constriction. Fig. 6e exhibits the velocity profile for several values of Weissenberg number. One can perceive that the magnitude of the velocity lessens with a surge in Weissenberg number because the inciting values of We increases the relaxation time of the fluid particles and thus enhance the viscosity even more which then creates resistance to the flow of blood as a consequence of the decrease in fluid's velocity.

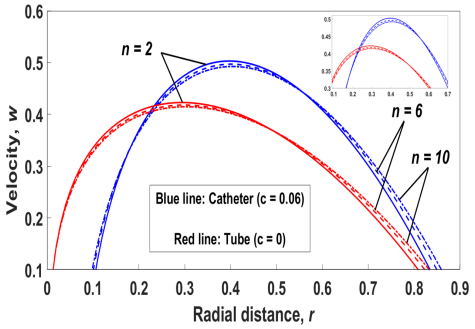

(a) Different n

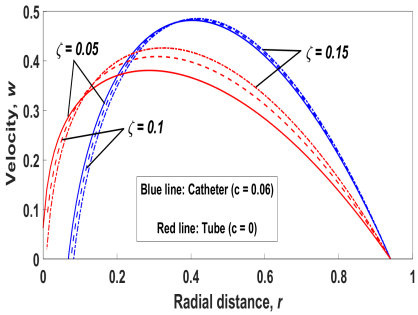

(b) Different ζ

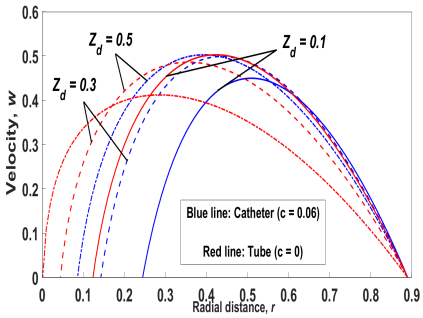

(c) Different z_d

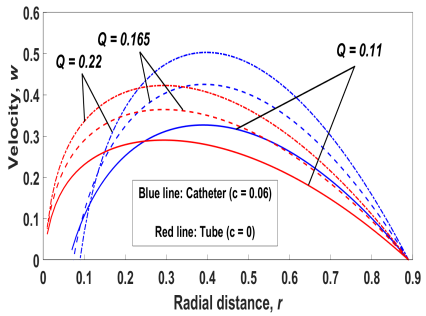

(d) Different Q

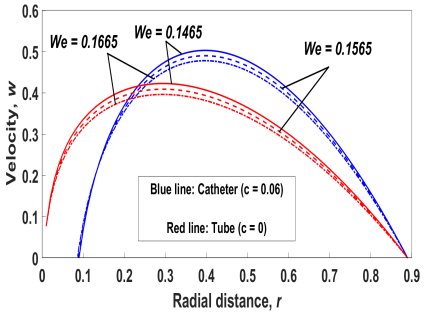

(e) Different We

Fig. 6. Velocity with radial distance for **(a)** several n values, **(b)** several ζ values, **(c)** several z_d values,**(d)** several Q values and **(e)** several We values with $R = 1, b = 1, a = 0, m = 2$ and $Gr = 5$

4.4 Wall shear stress/Skin friction

The graphs of skin friction with axial distance z are shown in Figs. 7a - 7f for several values of parameters (a) n, (b) ζ, (c) We, (d) δ, (e) Q and (f) z_d with $R = 1, b = 1, a = 0, m = 2, \beta = 0.5$ and $Gr = 5$. From Fig. 7a, one can note that as the parameter of the shape of stenosis n raises, the skin friction decreases up to mid axial distance and then it increases from the mid axial distance until it ends. The distribution of shear stresses at the wall of blood vessels is deeply influenced by the simultaneous existence of both stenosis and thrombosis in the artery.

Figs. 7b and 7c outlines the variation of skin friction axially for several values of the utmost height acquired by the clot and maximum depth of stenosis, respectively. In both cases, skin friction rises with increase in both parameters, i.e. the arterial wall experiences higher stress when stenosis grows deeper and in addition to the thrombosis growth. This further influence the wall shear stress to surge significantly which leads to the declining of blood movement in the artery.

Fig. 7d portrays the behavior of skin friction for different flow rate (Q) values. It is viewed that with the upsurge of flow rate, the shear stresses at the wall increases significantly. The significant increase is due to the simultaneous growth of stenosis and thrombosis which makes the artery to constrict even more. In Fig. 7e, the graph of skin friction for distinct values of Weissenberg number We has been plotted against axial distance z. It is spotted that by uplifting We, the skin friction coefficient lessens remarkably owing to the rise of inertial forces.

Fig. 7f compares the wall shear stress of Carreau and Newtonian fluids for different values of z_d. One can notice that when the blood clot axially moves from

0 to 0.2, the skin friction diminishes greatly and when it flows further from 0.2 to to 0.3, the skin friction reduces considerably as a consequence of the simultaneous attendance of constrictions (stenosis and clot) in the artery. It is pertinent to mention that the plot of wall shear stresses of Newtonian fluid model (obtained from Carreau fluid model when $We = 0$) is in favourable agreement with the complementary plot in Fig. 9a of Elnaqeeb et al. [6] and this validates the present study.

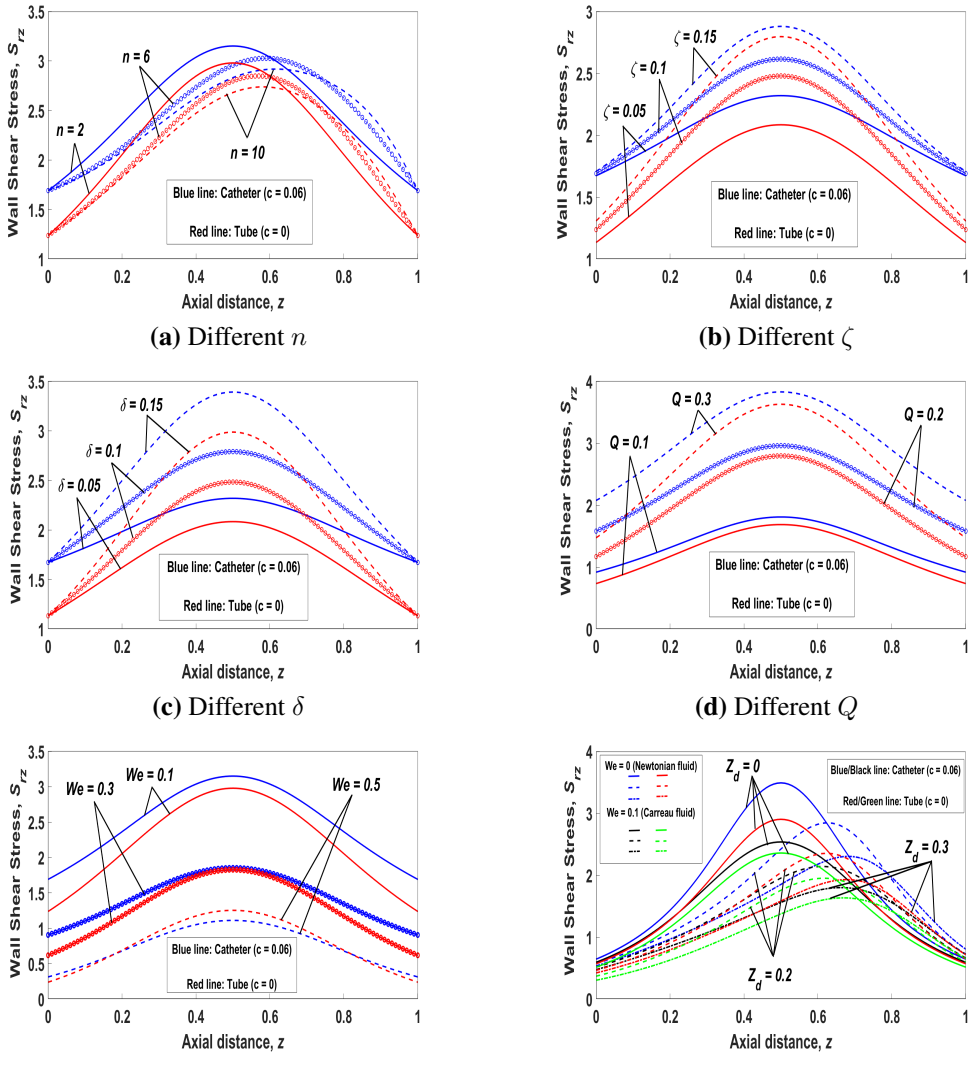

(a) Different n **(b)** Different ζ

(c) Different δ **(d)** Different Q

(e) Different We **(f)** Different z_d

Fig. 7. Shear stresses at the wall with axial distance for **(a)** several n values, **(b)** several ζ values, **(c)** several We values, **(d)** several δ values, **(e)** several Q values and **(f)** several z_d values with $R = 1, b = 1, a = 0, m = 2, \beta = 0.5$ and $Gr = 5$

4.5 Resistive Impedance

The graph of resistance to flow with utmost stenotic depth δ for several parameter values of the shape of stenosis n, are portrayed in Fig. 8a. It is perceived that the resistance diminishes inconsiderably with the rise in n for both tube and catheter. Fig. 8b demonstrates the variation of resistive impedance with δ for various height of the blood clot ζ. It reveals that as the clotting in the artery deepens, it reduces the flow of the blood and thus it raises the resistance to flow.

Fig. 8c depicts the impact of Weissenberg number We on the resistance to flow when it differs with highest stenotic depth δ. It is found that as We rises, the resistance to flow decreases substantially as a result of an increase in relaxation time which makes blood in the artery to move easily. Fig. 8d is sketched to analyze the consequences of z_d on the resistance to flow with maximum stenotic depth. We deduce that when z_d moves forward, the resistance decreases appreciably as a consequence of nanofluid's presence, i.e. the presence of nanofluid intensifies the motion of blood in the stenosed arteries containing clot.

Fig 8e displays the impact of flow rate variation with maximum stenotic depth on the resistive impedance. It is recorded that a slight rise in the flow rate (Q) results in the marginal reduction in the resistive impedance with the simultaneous existence of stenosis and blood clot.

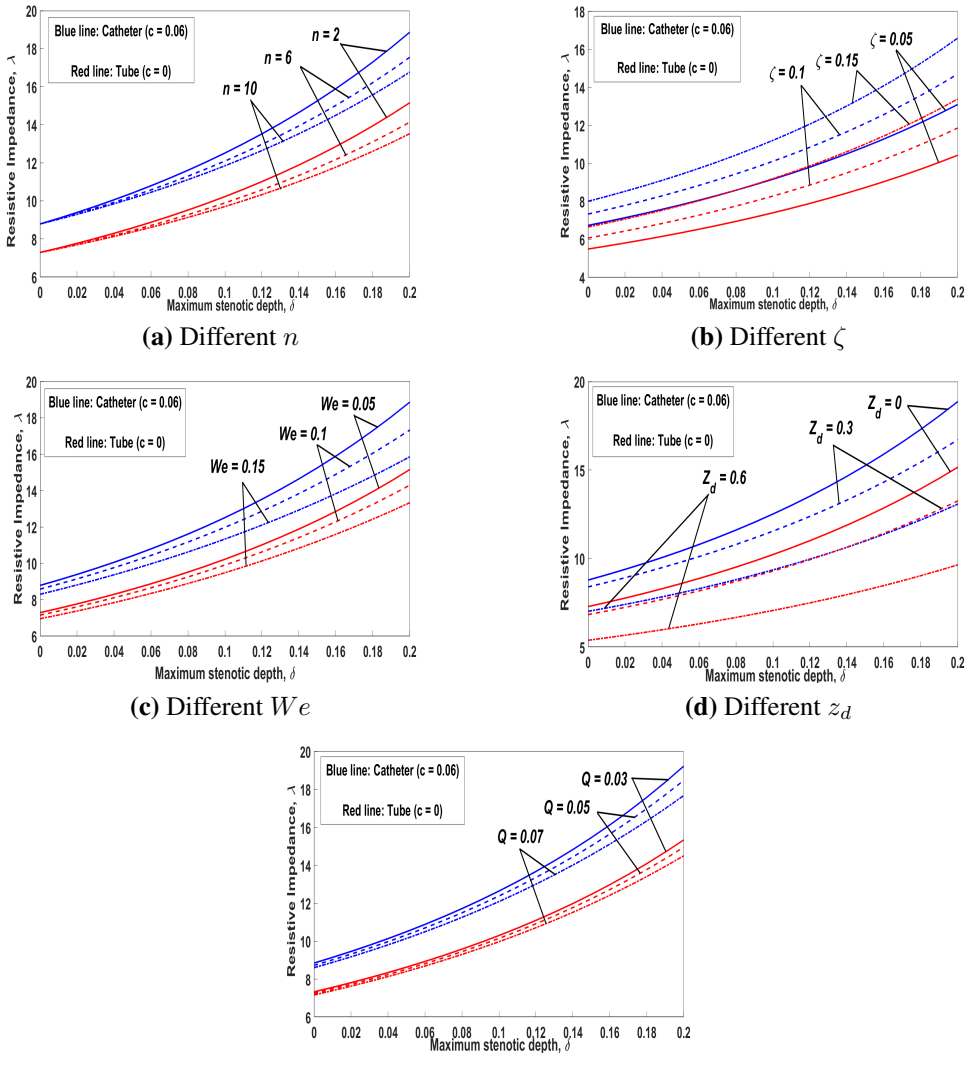

(a) Different n

(b) Different ζ

(c) Different We

(d) Different z_d

(e) Different Q

Fig. 8. Resistive Impedance with maximum stenotic depth for several **(a)** n values, **(b)** several ζ values, **(c)** several We values, **(d)** several z_d values and **(e)** several Q values with $R = 1, b = 1, a = 0, z = 0, m = 2, , Gr = 2$ and $\beta = 0.5$.

4.6 Streamlines

The stream lines are effective two-dimensional pictorial representation which can depict the motion of fluid particles, i.e., streamlines (of blood flow) are lines that are instantaneously tangent to the velocity vector of the fluid flow. Since it is impossible for a fluid particle to have two distinct velocities at once, streamlines cannot intersect. Figs. 9a - 9l exhibits the streamlines of blood flow which are drawn for distinct values of various parameters .

Figs. 9a and 9b show the pattern of blood flow for different height of blood clot, ζ. One can observe that as the clot grows, the streamlines converge towards the centre, indicating the phenomenon of thrombosis. The effects of catheter radius on the stream line pattern of blood flow are illustrated in Figs. 9c and 9d where the trapping phenomenon is lessened owing to the surge of the radius ratio of catheter c. This implies that the trapping bolus is more in the case of a tube model in comparison to the catheter model.

The influences of flow rate (Q) in the stream line of blood flow can be seen in Figs. 9e and 9f. The constriction grows significantly when the flow rate Q value raises from 0.02 to 0.07, the pressure rises to higher level due to the simultaneous development of stenosis and thrombosis. Figs. 9g and 9h outline the effects of varying the maximum stenotic depth δ on the streamlines. One can note that as δ ascends, the occurrence of stenosis is more critical as seen from the convergence of the streamlines towards the centre.

The variation of stenosis shape parameter n on streamlines are portrayed in Figs. 9i and 9j with $n = 2$ and $n = 6$, respectively. It is pertinent to mention that the skewness in the stream lines pattern are clearly noticed in Fig. 9j when

n increases from 2 to 6. It is known that n indicates the stenosis shape parameter and thus any increase of the parameter value will show skewness towards the right side and additionally, since blood clot occurs in the inner tube, one can see the narrow contour at the middle. Figs. 9k and 9l points out the consequences of Weissenberg number, We on streamlines. It is important to emphasize that a rise in the Weissenberg number We results in the lessening of pressure gradient as well as the rise of the relaxation time of the fluid and hence it produces a reduction in resistance to the fluid particles.

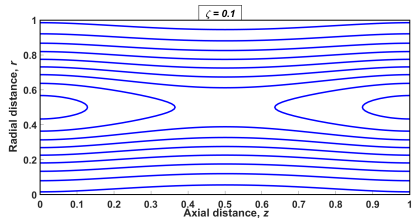

(a) Different ζ

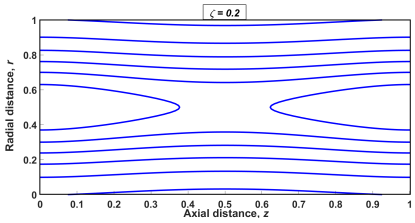

(b) Different ζ

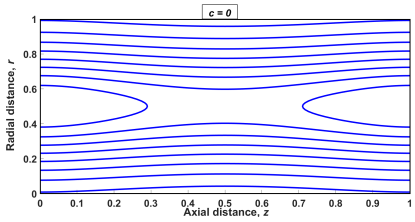

(c) Different c

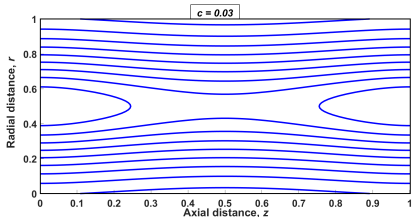

(d) Different c

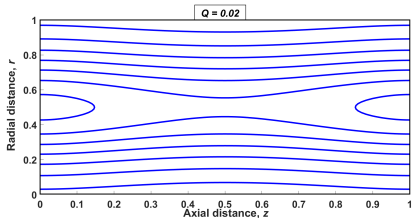

(e) Different Q

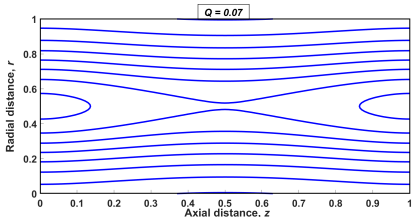

(f) Different Q

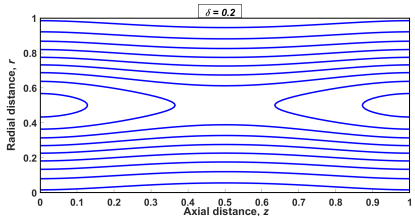

(g) Different δ

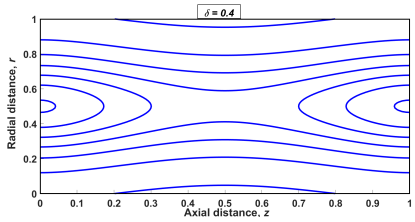

(h) Different δ

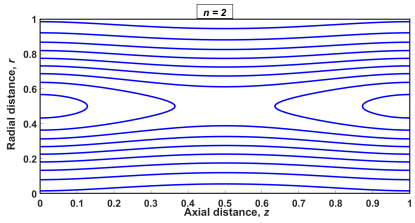

(i) Different n

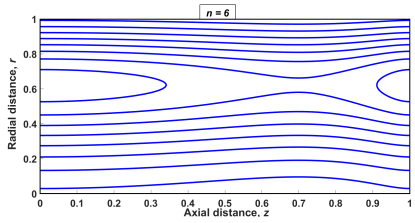

(j) Different n

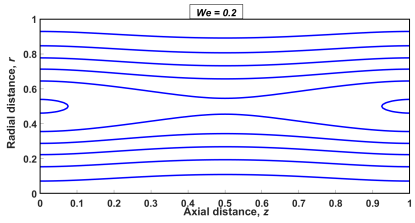

(k) Different We

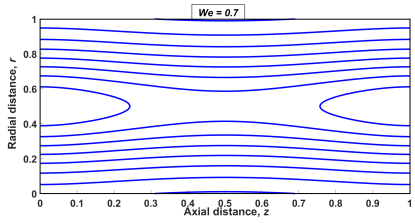

(l) Different We

Fig. 9. Streamlines pattern of the blood motion with $R = 1, b = 1, a = 0, m = 2, z_d = 0, Gr = 3$ and $\beta = 0.1$.

5 Clinical Applications

As a potential application of the current investigation to the field of medicine, Tables 3 - 7 compute the physiological data of pressure gradient, resistive impedance and skin friction for distinct types of catheter (Guidewire, Infusion and Angioplasty Catheter) and its radius are taken from [54, 55].

Table 3 presents the axial variation of pressure gradient for various types of catheters and different stenosis shape parameter n values; whereas Table 4 computes the pressure gradient axially for several values of z_d, axial displacement of the clot. It is observed that for all three types of catheter, the pressure gradient reduces with increasing stenosis shape parameter and z_d. The reduction in pressure gradient indicates the capability of catheters in alleviating blood flow in the constricted artery.

Table 3: Estimates of pressure gradient at different locations in the axial direction and for different types of catheters for different values of n with $R = 1, b = 1, a = 0, z_d = 0, m = 2, We = 0.5, Gr = 5, \beta = 0.5, \zeta = 0.1, \delta = 0.1$ and $Q = 0.985$.

Types of catheter	Range of catheter size	z	n = 2	n = 6	n = 10
Guidewire	**0.08 - 0.18**	0.2	1.17 - 1.32	1.08 - 1.23	1.07 - 1.21
		0.4	1.36 - 1.47	1.27 - 1.37	1.24 - 1.34
		0.6	1.36 - 1.47	1.36 - 1.46	1.32 - 1.43
		0.8	1.17 - 1.32	1.25 - 1.41	1.27 - 1.43
Infusion	**0.14 - 0.33**	0.2	1.27 - 1.43	1.18 - 1.33	1.17 - 1.31
		0.4	1.43 - 1.60	1.34 - 1.49	1.30 - 1.45
		0.6	1.43 - 1.60	1.43 - 1.59	1.39 - 1.55
		0.8	1.27 - 1.43	1.36 - 1.53	1.39 - 1.56
Angioplasty Catheter	**0.3 - 0.6**	0.2	1.41 - 2.13	1.31 - 1.79	1.29 - 1.75
		0.4	1.57 - 4.86	1.46 - 3.18	1.42 - 2.80
		0.6	1.57 - 4.86	1.56 - 4.78	1.52 - 4.06
		0.8	1.41 - 2.13	1.51 - 2.68	1.53 - 2.88

Table 4: Estimates of pressure gradient at different locations in the axial direction and for different types of catheters for different z_d values with $R = 1, b = 1, a = 0, n = 2, m = 2, We = 0.5, Gr = 5, \beta = 0.5, \zeta = 0.1, \delta = 0.1$ and $Q = 0.985$.

Types of catheter	Range of catheter size	z	$z_d = 0.2$	$z_d = 0.4$	$z_d = 0.6$
Guidewire	**0.08 - 0.18**	0.2	1.08 - 1.28	1.05 - 1.27	1.05 - 1.27
		0.4	1.26 - 1.42	1.17 - 1.39	1.14 - 1.37
		0.6	1.36 - 1.47	1.26 - 1.42	1.17 - 1.39
		0.8	1.26 - 1.36	1.26 - 1.36	1.17 - 1.32
Infusion	**0.14 - 0.33**	0.2	1.05 - 1.27	1.21 - 1.40	1.21 - 1.40
		0.4	1.17 - 1.39	1.32 - 1.52	1.31 - 1.51
		0.6	1.26 - 1.42	1.37 - 1.55	1.32 - 1.52
		0.8	1.26 - 1.36	1.32 - 1.47	1.27 - 1.43
Angioplasty Catheter	**0.3 - 0.6**	0.2	1.38 - 1.84	1.38 - 1.84	1.05 - 1.27
		0.4	1.52 - 2.78	1.50 - 2.26	1.49 - 2.18
		0.6	1.57 - 4.86	1.52 - 2.78	1.50 - 2.26
		0.8	1.44 - 3.02	1.44 - 3.02	1.41 - 2.13

The estimates of the resistance to flow at different locations in the axial direction, various types of catheters (Guidewire, Infusion and Angioplasty Catheter) and also for several values of Weissenberg number We are presented in Table 5. Here, the axial distance, z are shown only until $z = 0.5$ due to the symmetric pattern of the stenosis considered in this case. One can notice that an upsurge in Weissenberg number causes a reduction in the resistive impedance for all three types of catheter although an increase in z gives rise to the elevation in resistive impedance. As the relaxation time raises, the enhancement of blood flow is achieved and by incorporating the catheter to further intensify the motion of blood reduces the resistive impedance.

Table 6 computes the estimates of the resistive impedance at different positions in the axial direction and for several kinds catheters and also for distinct values of varying height of blood clot ζ. As in Table 5, the estimates of resistive impedance are also computed upto $z = 0.5$. The development of clot in the mild stenosed artery leads to the escalation in resistance to flow. One can record that

the incorporation of catheter results in greater notable rise in the magnitude of resistive impedance, in addition to that of stenosis and thrombus in the artery.

Table 5: Estimates of resistive impedance at different locations in the axial directions and for different types of catheters for different We values with $R = 1, b = 1, a = 0, z_d = 0, m = 2, n = 2, Gr = 2, \beta = 0.5, \zeta = 0.15, \delta = 0.05$ and $Q = 0.05$.

Types of catheter	Range of catheter size	z	$We = 0.3$	$We = 0.5$	$We = 0.7$
Guidewire	**0.08 - 0.18**	0.1	6.60 - 8.36	5.54 - 6.84	4.80 - 5.85
		0.3	8.84 - 10.78	7.23 - 8.51	6.18 - 7.15
		0.5	10.05 - 12.01	8.09 - 9.32	6.86 - 7.76
Infusion	**0.14 - 0.33**	0.1	7.67 - 10.86	6.37 - 8.38	5.48 - 6.96
		0.3	10.02 - 13.58	8.04 - 10.19	6.80 - 8.36
		0.5	11.25 - 15.00	8.86 - 11.13	7.43 - 9.07
Angioplasty Catheter	**0.3 - 0.6**	0.1	10.36 - 16.83	8.08 - 12.19	6.75 - 9.83
		0.3	13.00 - 24.20	9.84 - 17.38	8.10 - 13.95
		0.5	14.35 - 35.75	10.73 - 25.61	8.78 - 20.54

Table 6: Estimates of resistive impedance at different locations in the axial direction and for different types of catheters for different ζ values with $R = 1, b = 1, a = 0, z_d = 0, m = 2, n = 2, Gr = 2, \beta = 0.5, \delta = 0.05, We = 0.5$ and $Q = 0.05$.

Types of catheter	Range of catheter size	z	$\zeta = 0.05$	$\zeta = 0.1$	$\zeta = 0.15$
Guidewire	**0.08 - 0.18**	0.1	5.08 - 6.36	5.23 - 6.47	5.38 - 6.58
		0.3	5.85 - 7.12	6.32 - 7.48	6.74 - 7.83
		0.5	6.24 - 7.48	6.90 - 8.01	7.48 - 8.52
Infusion	**0.14 - 0.33**	0.1	5.89 - 7.86	6.02 - 7.96	6.14 - 8.05
		0.3	6.65 - 8.66	7.05 - 9.01	7.42 - 9.37
		0.5	7.02 - 9.03	7.59 - 9.58	8.11 - 10.19
Angioplasty Catheter	**0.3 - 0.6**	0.1	7.57 - 11.23	7.67 - 11.44	7.77 - 11.68
		0.3	8.36 - 12.83	8.70 - 14.01	9.05 - 15.77
		0.5	8.72 - 13.81	9.25 - 16.45	9.82 - 24.39

Table 7 assesses the rates of increase in skin friction for distinct values of catheter radius ratio, c and for several locations of blood clot z_d. These estimates clearly measures the impacts of catheterization on the wall shear stress of the fluid flow. It is clear that there is a considerable rise in the shear stresses at the wall

for the contemporary Carreau fluid model when the radius of the catheter rises. Another important thing to note is the marginal drop in the magnitude of wall shear stress when the blood clot moves forward in the axial direction.

Table 7: The estimates of increase in skin friction for different catheter radius ratio c and for various values of axial position of blood clot, z_d with $R = 1, b = 1, a = 0, m = 2, z = 0, We = 0.5, Gr = 2, \beta = 0.5, \zeta = 0.1, \delta = 0.1$ and $Q = 0.22$.

Ratio of increase in the skin friction for different catheter radius				
c	$z_d = 0.025$	$z_d = 0.05$	$z_d = 0.075$	$z_d = 0.1$
0.04	2.91	2.65	2.32	1.91
0.06	3.2	3.08	2.91	2.69
0.08	3.95	3.92	3.86	3.77
0.1	3.98	4.95	4.97	4.97

6 Discussion of Results

In this present study, the method of perturbation is employed for solving the resulting non-linear differential equations as it provides analytical solutions to various flow quantities.Approximate solutions are acquired through the expansion of the unknown variable viz., velocity in perturbation series in terms of small parameter Weissenberg number (time-dependent parameter) We.

In the interest of understanding the physical features of blood movement in a stenosed catheterized artery with thrombosis, the immense quantitative analysis is executed numerically by the extensive utilization of MATLAB/MATHEMATICA softwares and are exhibited both tabularly and graphically. From Figs. 6a - 6e, one can deduce that as the constriction develops mildly as a result of both stenosis and thrombosis, the velocity decreases which reduces the motion of blood in the

artery. The identical character can be seen when Weissenberg number surges. This is caused by the rise in relaxation time of the blood particles which intensifies the blood viscosity even more and thus, it raises frictional resistance to the flow. However, when blood clot position displaces further, the velocity increases on account of the narrowed blood vessels when the value of Q increases in both situations (tube and catheter).

Skin friction is another key rheological quantity which discovers the impacts of thrombosis and stenosis in an artery. It plays a fundamental role not only in the evolution of atherosclerotic plaque, but also to influence the vulnerability in the normal blood circulation. Figs 7a - 7f discloses the fact that the rise in the skin friction influences the formation of thrombus where it harms the wall of the vessel and creates intimal thickening which triggers aggregation of platelets. It is prominent to highlight that the magnitude of shear stresses at the wall increases with increasing flow rate and stenosis depth owing to the enlargement of plaque at the arterial wall. This also indicates that the simultaneous existence of stenosis and thrombosis greatly enhances the wall shear stress. The decline in the magnitude of skin friction is caused by the increase in We where the ratio of the relaxation time of the fluid soars and hence makes the blood to move smoothly. The primary cause of the increase in the value of skin friction with the rise of the flow rate is due to the ”no slip condition” at the boundary of the artery.

The graphical results presented in Figs 8a - 8e demonstrate the influence of various parameters on resistance to flow which reveals that the reduction in resistive impedance is seen as a consequence of the surge in stenosis shape parameter and the reverse is noticed when the height of blood clot boosted. It is recorded that as the thrombus develops in the artery, it lessens the flow of blood and thus

surges the resistance to flow. We may also perceive that the magnitude of resistive impedance enhances when there is a decline in We which increases the velocity field and creates impedance to the flow of blood. Ultimately, it can also be mentioned that when the height of the stenosis grows, the resistive impedance to flow increases at the wall.

From the physiological data provided in Tables 3-6, it is worth noting that both pressure gradient and resistive impedance are the increasing functions of Angioplasty catheter. One can infer that the implementation of Angioplasty catheter helps in improving flow of blood significantly in comparison to Guidewire and Infusion catheters as it utilizes a balloon-tipped catheter to unclog the blocked blood vessels. In general, as the radius of the catheter increases, the pressure distribution and the resistive impedance raise as a result of the shrinkage of the annular region of the artery. It is also pertinent to mention that the increase in relaxation time (We) which escalates the motion of blood and catheterization in the stenosed artery with thrombosis rises the frictional resistance in the blood flow. Due to the wider usage of catheters clinically, the presented estimations might be useful to physicians in deciding their ensuing course of action.

7 Conclusion

In the present study, the steady incompressible axisymmetric flow of metallic nanoparticles suspended blood flow via stenosed catheterized artery with thrombosis is investigated, modelling blood as non-Newtonian Carreau fluid. The governing equations of motion are solved by employing the regular perturbation method. MATLAB/MATHEMATICA softwares are comprehensively used to create and

execute codes in order to generate the data which are then exhibited in graphical and tablular forms for further analysis. The influences of stenosis shape pareameter, maximum depth attained by stenosis and maximum height of blood clot, Weissenberg number, axial displacement of the clot and flow rate on temperature, pressure gradient, velocity, shear stresses at the wall and resistive impedance to flow are analyzed. The major findings of this study are compiled below:

- Temperature of the fluid lessens with the increase in stenosis shape parameter and depth of stenosis which results in the reduction of flow of blood in the artery.
- When the stenotic depth and blood clot thickens, pressure gradient surges as a result of the increasing constriction in the artery and thus needs assistance such as pressure to push blood from the upstream.
- Pressure gradient is also found to increase when the flow rate, Q increases.
- The rise in Weissenberg number reduces the velocity distribution, owing to the rise in relaxation time of the fluid which intensifies the viscosity and hence raises the frictional resistance to blood flow.
- When the position of blood clot displaces, velocity increases considerably and the same behaviour is noted when the flow rate surges.
- The magnitude of resistance to blood flow reduces with the upsurge of flow rate and stenosis shape parameter. The reverse character is recognized when Weissenberg number, the depth and axial displacement of blood clot increases.

- A rise in Weissenberg number results in the significant reduction in the magnitude of skin friction due to the rise in inertial forces.

- The ratio of increase in the skin friction raises slightly with the rise of different catheter radius and the forward movement of blood clot in the axial direction.

- When the catheter guidewire radius is 0.18, the pressure gradient in blood flow is observed to differ in the range of $1.21 - 1.43$ with the axial variation of $0.2 - 0.8$ and found to decrease from $1.36 - 1.32$ when the blood clot position shifted from 0.2 to 0.6.

- When the angioplasty catheter of radius 0.3 is used, the resistance to flow surges considerably in the range of $6.75 - 8.78$ when z varies from 0.1 to 0.3 with $We = 0.7$.

From the obtained fascinating theoretical results and the clinical applications, it is hoped that this contemporary mathematical model could be very useful to the medical practitioners in predicting the nature of the movement of blood in stenotic catheterized artery with thrombus formation. The current work shall further be developed to pulsatile motion of blood with the incorporation of body acceleration and magnetic field in order to produce a more practical model. It is also planned to mathematically investigate the flow of blood in a cardiovascular system with stenting, a modern technique for treating the abnormalities of aneurysm and stenosis.

Funding

Not applicable.

Conflict of interest

The authors declare that they have no competing interests.

Availability of data and material

Not applicable.

Code availability

Not applicable.

Authors' contributions

AWS perceived the research problem, formulated it as mathematical model and contributed in obtaining the analytical solutions and also take part in developing MATLAB code for generating data for plotting the graphs and then analyzing the results. DSS contributed in obtaining the expressions for rheological quantities

and involved in generating the data for plotting the graphs through MATLAB programming and analysed and validated the results. AKN analysed and validated the results. All authors read and approved the final manuscript.

References

1. Sweed, N., Mekheimer, K.S., EL-Kholy, A., Abdelwahab, A.: Alterations in pulsatile bloodstream with the heat and mass transfer through asymmetric stenosis artery: Erythrocytes suspension model. Heat Transf. **50**(3), 2259-2287 (2021)

2. Ponalagusamy, R.: Blood flow through stenosed tube. Ph.D. Dissertation, Ph.D Thesis, IIT, Bombay, India (1986)

3. Liepsch, D., Singh, M., Lee, M.: Experimental analysis of the influence of stenotic geometry on steady flow. Biorheol. **29**(4), 419–431 (1992)

4. Al-Saad, M., Suarez, C., Obeidat, A., Bordas, S., Kulasegaram, S.: Application of smooth particle hydrodynamics method for modelling blood flow with thrombus formation. Comput. Model Eng. Sci. **122**(3), 831–862 (2020)

5. Jackson, S.P.: Arterial thrombosis—insidious, unpredictable and deadly. Nat. Med. **17**(11), 1423–1436 (2011)

6. Elnaqeeb, T., Mekheimer, K.S., Alghamdi, F.: Cu-blood flow model through a catheterized mild stenotic artery with a thrombosis. Math. Biosci. **282**, 135–146 (2016)

7. Young, D.F., Tsai, F.Y.: Flow characteristics in models of arterial stenoses—i. steady flow. J. Biomech. **6**(4), 395–410 (1973)

8. MacDonald, D.: On steady flow through modelled vascular stenoses. J. Biomech. **12**(1), 13–20 (1979)

9. Chaturani, P., Samy, R. P.: Pulsatile flow of casson's fluid through stenosed arteries with applications to blood flow. Biorheol. **23**(5), 499–511 (1986)

10. Afiqah, W.S., Sankar, D.S.: Effects of porosity in four-layered non-linear blood rheology in constricted narrow arteries with clinical applications. Comp. Meth. Prog. Bio. **199**(105907), (2021).

11. Kumawat, C., Sharma, B.K., Mekheimer, K.S.: Mathematical analysis of two-phase blood flow through a stenosed curved artery with hematocrit and temperature dependent viscosity. Phys. Scr., IOP Publishing.**96**(12), 125277 (2021)

12. Karino, T., Goldsmith, H.L.: Flow behaviour of blood cells and rigid spheres in an annular vortex. Philosophical Transactions of the Royal Society of London, B, Biol. Sci. **279**(967), 413–445 (1977)

13. Kapur, J.N.: Mathematical models in Biology and Medicine. East-West Press Pvt. Ltd., New Delhi, India, (1992).

14. Mann, K.G., Butenas, S., Brummel, K.: The dynamics of thrombin formation. Arterioscler. Thromb. Vasc. Biol. **23**(1), 17–25 (2003)

15. Sankar, D.S.: Two-phase non-linear model for blood flow in asymmetric and axisymmetric stenosed arteries. Int. J. Non Linear Mech. **46**(1), 296–305 (2011)

16. Choi, S.U.: Nanofluids: from vision to reality through research. J. Heat Trans. **131**(3) (2009)

17. Tyler, T., Shenderova, O., Cunningham, G., Walsh, J., Drobnik, J., McGuire, G.: Thermal transport properties of diamond-based nanofluids and nanocomposites. Diam. Relat. Mater. **15**(11-12), 2078–2081 (2006)

18. Das, S.K., Choi, S.U., Patel, H.E.: Heat transfer in nanofluids—a review. Heat Transf. Eng. **27**(10), 3–19 (2006)

19. Liu, M.S., Lin, M.C.C., Huang, I.T., Wang, C.C.: Enhancement of thermal conductivity with carbon nanotube for nanofluids. Int. Commun. Heat Mass Transf. **32**(9), 1202–1210 (2005)

20. Nsofor, E.C.: Recent patents on nanofluids (nanoparticles in liquids) heat transfer. Recent Pat. Mech. Eng. **1**(3), 190–197 (2008)

21. Afiqah, W.S., Sankar, D.S.: Two-phase nonlinear rheological analysis of blood flow in small diameter blood vessels with constriction. ARPN J. Eng. Appl. Sci. **15**(10), 1129–1143 (2020)

22. Khan, M.I., Alzahrani, F., Hobiny, A.: Heat transport and nonlinear mixed convective nanomaterial slip flow of walter-b fluid containing gyrotactic microorganisms. Alex. Eng. J. **59**(3) 1761–1769 (2020)

23. Bugliarello, G., Hayden, J.W.: Detailed characteristics of the flow of blood in vitro. Trans. Soc. Rheol. **7**(1), 209–230 (1963)

24. Bugliarello, G., Sevilla, J.: Velocity distribution and other characteristics of steady and pulsatile blood flow in fine glass tubes. Biorheol. **7**(2), 85–107 (1970)

25. Cokelet, G.: The rheology of human blood. in: Biomechanics: Its foundations and objectives (1972)

26. Shukla, J., Parihar, R., Rao, B.: Effects of stenosis on non-newtonian flow of the blood in an artery. Bull. Math. Biol. **42**(3), 283–294 (1980)

27. Priyadharshini, S., Ponalagusamy, R.: Computational model on pulsatile flow of blood through a tapered arterial stenosis with radially variable viscosity and magnetic field. Sadhana **42**(11), 1901–1913 (2017)

28. Yilmaz, F., Gundogdu, M.Y.: A critical review on blood flow in large arteries; relevance to blood rheology, viscosity models, and physiologic conditions. Korea Aust. Rheol. J. **20**(4), 197–211 (2008)

29. Zaman, A., Ali, N., B´eg, O.A.: Unsteady magnetohydrodynamic blood flow in a porous-saturated overlapping stenotic artery—numerical modeling. J. Mech. Med. Biol. **16**(4), 1650049 (2016)

30. Haghighi, A.R., Asl, M.S., Kiyasatfar, M: Mathematical modeling of unsteady blood flow through elastic tapered artery with overlapping stenosis. J. Braz. Soc. Mech. Sci. **37**(2), 571–578 (2015)

31. Barnes, H.A., Hutton, J.F., Walters, K.: An introduction to rheology. Elsevier **3** (1989).

32. Zaman, A., Ali, N., Sajid, M., Hayat, T.: Effects of unsteadiness and nonnewtonian rheology on blood flow through a tapered time-variant stenotic artery. AIP Adv. **5**(3), 037129 (2015)

33. Nadeem, S., Ijaz, S., Akbar, N.S.: Nanoparticle analysis for blood flow of prandtl fluid model with stenosis. Int. Nano Lett. **3**(1), 1–13 (2013)

34. Ellahi, R., Rahman, S., Nadeem, S., Akbar, N.S.: Blood flow of nanofluid through an artery with composite stenosis and permeable walls. Appl. Nanosci. **4**(8), 919–926 (2014)

35. Ahmed, A., Nadeem, S.: The study of (cu, tio2, al2o3) nanoparticles as antimicrobials of blood flow through diseased arteries, J. Mol. Liq. **216**, 615–623 (2016)

36. Mekheimer, K.S., Elnaqeeb, T., El Kot, M., Alghamdi, F.: Simultaneous effect of magnetic field and metallic nanoparticles on a micropolar fluid through an overlapping stenotic artery: blood flow model. Phys. Essays **29**(2), 272–283 (2016)

37. Mekheimer, K.S., Mohamed, M.S., Elnaqeeb, T.: Metallic nanoparticles influence on blood flow through a stenotic artery. Int. J. Pure. Appl. Math. **107**(1), 201 (2016)

38. Nadeem, S., Ijaz, S.: Influence of metallic nanoparticles on blood flow through arteries having both stenosis and aneurysm. IEEE Trans. Nanobiosci. **14**(6), 668–679 (2015)

39. Akbar, N.S.: Metallic nanoparticles analysis for the blood flow in tapered stenosed arteries: Application in nanomedicines. Int. J. Biomath. **9**(1), 1650002 (2016)

40. Nadeem, S., Ijaz, S.: Study of radially varying magnetic field on blood flow through catheterized tapered elastic artery with overlapping stenosis. Commun. Theor. Phys. **64**(5), 537 (2015)

41. Zidan, A., McCash, L., Akhtar, S., Saleem, A., Issakhov, A., Nadeem, S.: Entropy generation for the blood flow in an artery with multiple stenosis having a catheter. Alex. Eng. J. **60**(6), 5741–5748 (2021)

42. Ramadan, S.F., Mekheimer, Kh.S., Bhatti, M.M., Moawad, A.M.A.: Phan-thien-tanner nanofluid flow with gold nanoparticles through a stenotic electrokinetic aorta: A study on the cancer treatment. Heat Transf. Res. **52**(16), (2021)

43. Elogail, M.A., Mekheimer, Kh.S.: Modulated viscosity-dependent parameters for MHD blood flow in microvessels containing oxytactic microorganisms and nanoparticles. Symmetry. **12**(12), 2114 (2020)

44. Zhang, L., Bhatti, M.M., Marin, M., Mekheimer Kh.S.: Entropy analysis on the blood flow through anisotropically tapered arteries filled with magnetic zinc-oxide (ZnO) nanoparticles. Entropy. **22**(10), 1070 (2020)

45. Abdelsalam, S.I., Mekheimer, Kh.S., Zaher, A.Z.: Alterations in blood stream by electroosmotic forces of hybrid nanofluid through diseased artery: aneurysmal/stenosed segment. Chin. J. Phys. **67**, 314-329 (2020)

46. Ramadan, S.F., Mekheimer, Kh.S.: New Insight into Gyrotactic Microorganisms in Anti-Infection Agents Through Wavy Deformable Catheter/Endoscope with Non-Linear Thermal Radiation: Numerical Study. J. Adv. Res. Fluid Mech. Therm. Sci. **75**(3), 25-42 (2020)

47. Ijaz, S., Nadeem, S.: Transportation of nanoparticles investigation as a drug agent to attenuate the atherosclerotic lesion under the wall properties impact. Chaos Solitons Fractals. **112**, 52-65 (2018)

48. Nadeem, S., Fuzhang, W., Alharbi, F.M., Sajid, F., Abbas, N., El-Shafay, A.S., Al-Mubaddel, F.S.: Numerical computations for Buongiorno nano fluid model on the boundary layer flow of viscoelastic fluid towards a nonlinear stretching sheet. Alex. Eng. J. **61**(2), 1769-1778 (2022)

49. Ahmad, S., Khan, M.N., Nadeem, S.: Unsteady three dimensional bioconvective flow of Maxwell nanofluid over an exponentially stretching sheet with variable thermal conductivity and chemical reaction. Int. J. Ambient. 1-11 (2022)

50. Muhammad, N., Nadeem, S., Khan, U., Sherif, El-Sayed M., Issakhov, A.: Insight into the significance of Richardson number on two-phase flow of ethylene glycol-silver nanofluid due to Cattaneo-Christov heat flux. Waves Random Complex Media. 1-19 (2021)

51. Nadeem, S., Haq, R.U., Khan, Z.H.: Heat transfer analysis of waterbased nanofluid over an exponentially stretching sheet. Alex. Eng. J. **53**(1), 219–224 (2014)

52. Nadeem, S., Ijaz, S.: Theoretical analysis of metallic nanoparticles on blood flow through stenosed artery with permeable walls. Phys. Lett. A. **379**(6), 542–554 (2015)

53. Sheikholeslami, M., Ganji, D.D., Javed, M.Y., Ellahi, R.: Effect of thermal radiation on magnetohydrodynamics nanofluid flow and heat transfer by means of two phase model. J. Magn. Magn. Mater. **374**, 36–43 (2015)

54. Back, L.: Estimated mean flow resistance increase during coronary artery catheterization. J. Biomech. **27**(2), 169–175 (1994)

55. Sankar, D.S.: A two-fluid model for pulsatile flow in catheterized blood vessels. Int. J. Non Linear Mech. **44**(4), 337–351 (2009)